THE ASTROPHYSICAL JOURNAL, 424:793–799, 1994 April 1

MOLECULAR OUTFLOWS FROM FU ORIONIS STARS

NEAL J. EVANS II AND STEPHEN BALKUM
Department of Astronomy, The University of Texas at Austin, Austin, TX 78712-1083; I: nje@astro.as.utexas.edu
RUSSELL M. LEVREAULT
35 Payson Avenue, Easthampton, MA 01027
AND
LEE HARTMANN AND SCOTT KENYON
Harvard-Smithsonian Center for Astrophysics, 60 Garden Street, Cambridge, MA 02138
Received 1993 June 1; accepted 1993 October 5

ABSTRACT

We have detected molecular outflows toward six out of eight FU Orionis stars that we observed in the $J = 3 \rightarrow 2$ line of CO. Notably, FU Orionis itself does not show an outflow. Four of the souces were mapped, and two show evidence for multiple outflows. In both Z CMa and RNO 1b, nearby infrared sources may also be driving the outflows. Mass-loss rates derived from the usual assumptions of momentum conservation range from $3 \times 10^{-8}\ M_\odot\ \mathrm{yr}^{-1}$ to $2 \times 10^{-6}\ M_\odot\ \mathrm{yr}^{-1}$ without corrections for optical depth in the CO lines. Corrections for optical depth raise these estimates by a factor of 5 on average. If the outflows are driven by repeated outbursts with peak mass-loss rates of $10^{-5}\ M_\odot\ \mathrm{yr}^{-1}$, a duty cycle of 10^{-3} to 10^{-1} would be implied, consistent with other recent evidence.

Subject headings: ISM: jets and outflows — ISM: molecules — stars: variables: other (FU Orionis)

1. INTRODUCTION

The class of FU Orionis stars was originally characterized by a pre–main-sequence star which increased rapidly in visible brightness by 5 mag, followed by a slow decay. This event can be explained by a sudden increase in the accretion rate on a central T Tauri star, probably occasioned by instabilities in a massive disk (Kenyon, Hartmann, & Hewett 1988, and references therein). Models of thermal instabilities in accretion disks can explain the basic features of the FU Orionis phenomenon (Bell & Lin 1993). The massive disks can also explain a distinctive spectroscopic feature of these objects, strong absorption in the CO vibrational bands (in contrast to CO emission, which is more commonly seen toward young stars). Using this spectroscopic criterion, the class of FU Orionis stars expanded from five to nine (Hartmann, Kenyon, & Hartigan 1993).

P Cygni profiles of strong optical lines indicate that the rapid disk accretion (up to $\dot{M}$ of $10^{-3}\ M_\odot\ \mathrm{yr}^{-1}$) is accompanied by a strong disk wind with mass-loss rates of $\dot{M} \sim 10^{-5}\ M_\odot\ \mathrm{yr}^{-1}$ (Croswell, Hartmann, & Avrett 1987; Calvet, Hartmann, & Kenyon 1993). It has been suggested that the outbursts of FU Orionis objects cause highly time-dependent mass loss, which is responsible for exciting many Herbig-Haro objects (Reipurth 1990 and references therein). Thus study of FU Orionis winds is likely to be very important to an understanding of bipolar flows.

Despite the success of the disk interpretation in our understanding of these objects, many questions remain. One would like to know if the outburst initiates mass loss or whether it follows a period of sustained mass loss at a lower rate. Statistical arguments suggest that the outbursts must be repetitive, but the timescale and duty cycle (fraction of time spent in outburst) is poorly constrained.

Molecular outflows can provide information on these questions. Since current outbursts would not have had time to sweep up a detectable molecular outflow, detection of such an outflow implies that mass loss, either in a steady wind or in previous bursts, must have preceded the current episode. The size of the outflow divided by a characteristic velocity gives the lifetime of the outflow, shedding light on the age of the object and, if the outflow occurs only in bursts, the repetition timescale. Finally, a map of the outflow, combined with ^{13}CO data to constrain the optical depth, allows us to determine the momentum in the outflow. Assuming the flows are swept up by a faster ($v_{\mathrm{wind}} \sim 300\ \mathrm{km\ s}^{-1}$) stellar wind, momentum conservation allows us to compute the mass-loss rate, averaged over the lifetime of the outflow (Levreault 1988a). Division of the average $\dot{M}$ by the $\dot{M}$ determined in the outburst stage gives the duty cycle if all mass loss occurs in outbursts, or an upper limit to the duty cycle if mass loss occurs between outbursts.

We have surveyed eight FU Orionis stars for outflows. We did not include L1551 IRS 5 in our survey since it is well-studied. We did include some others previously observed in order to improve on the data. After we completed our survey, a 10th source, Parsamyan 21, was suggested to be a member of the class (Staude & Neckel 1992), and Strom & Strom (1993) have recently suggested two more candidates in L1641.

2. OBSERVATIONS AND REDUCTION

The objects were observed over five different observing runs at the Caltech Submillimeter Observatory (CSO)[1] on Mauna Kea in Hawaii. The search for wings was conducted using an SIS receiver, tuned to observe the $J = 3 \rightarrow 2$ line of CO at 345.7960 GHz. When a wing was seen, the source was mapped using a 20″ grid to determine the extent of the wing emission; typically, the rms noise in each spectrum of the map was 0.3 K. To distinguish wings from secondary velocity components and to assess optical depths, observations were made of the $J = 2 \rightarrow 1$ line of CO and the $J = 3 \rightarrow 2$ and/or the $2 \rightarrow 1$ lines

[1] The CSO is operated by the California Institute of Technology under funding from the National Science Foundation, contract AST 90-15755.

TABLE 1

SOURCE LIST

Source	α (1950)	δ (1950)	Off Position ('E, 'N)	Observation Date	Line
V346 Nor	$16^h28^m56^s.8$	−44°49'08"	(20, 20)	1990 Jul 18	^{12}CO 3–2
				1991 Apr 10	^{12}CO 3–2
				1992 Aug 12	^{13}CO 2–1
V1515 Cyg	20 22 03.0	+42 02 40	(60, −60)	1991 Oct 1	^{12}CO 3–2
				1992 Aug 12	^{13}CO 2–1
V1057 Cyg	20 57 06.2	+44 03 47	(−4, 4)	1991 Apr 10	^{12}CO 3–2
				1991 Oct 1	^{12}CO 3–2
Elias 1-12	21 45 26.9	+47 18 08	(−5, 5)	1991 Oct 1	^{12}CO 3–2
				1992 Aug 12	^{12}CO 2–1
					^{13}CO 2–1
					C^{18}O 2–1
RNO 1b	00 33 52.1	+63 12 24	(0, 20)	1991 Oct 1	^{12}CO 3–2
				1992 Feb 6	^{13}CO 3–2
FU Ori	05 42 38.2	+09 03 02	(0, 15)	1991 Oct 1	^{12}CO 3–2
Z CMa	07 01 22.6	−11 28 36	(0, −10)	1991 Oct 1	^{12}CO 3–2
				1992 Feb 6	^{13}CO 3–2
BBW 76	07 48 40.3	−32 58 43	(10, 0)	1991 Oct 1	^{12}CO 3–2

of ^{13}CO, depending on the source and receiver availability. Table 1 lists the sources, their positions, the off-source positions used for position-switching, the dates of observation, and the lines observed.

The backends were acousto-optic spectrometers with total bandwidths of both 50 and 500 MHz, the former resulting in velocity resolutions of about 0.085 km s^{-1} for the $J = 3 \rightarrow 2$ line of CO and 0.13 km s^{-1} for the $J = 2 \rightarrow 1$ line.

The pointing was checked regularly using planets or the $J = 3 \rightarrow 2$ emission from CO in circumstellar shells around evolved stars, such as CRL 618, CRL 2688, and o Ceti. The pointing generally repeated within an rms dispersion of 4"–5". Intensity calibration was achieved with an ambient temperature chopper wheel, thus providing data on the T_A^* scale. The beam size was about 20" for the $J = 3 \rightarrow 2$ transitions and about 30" for the $J = 2 \rightarrow 1$ transitions. The data must be corrected for power outside the main beam but not terminated at ambient temperature by dividing by the main beam efficiency; we used $\eta_{mb} = 0.55$ for $J = 3 \rightarrow 2$ line and 0.71 for the $J = 2 \rightarrow 1$ line, determined by measurements of Jupiter and Mars (Mangum 1993).

After calibration, a baseline was fitted and removed from each scan; velocities where emission was seen were excluded from the fit. Most scans required only a first-order baseline. One (V1515 Cyg) required a second-order baseline. For sources with previously published data, our spectra are reasonably consistent, but they often show wings not seen in previous spectra of lower J transitions with bigger beams.

3. RESULTS

Of the eight sources we surveyed, wings were found toward six. Including L1551 IRS 5, this brings the detection rate of wings toward FU Orionis stars to seven of nine, assuming that all the wings represent molecular outflows from the stars. The two sources without discernible wings are FU Ori itself (rms = 0.06 K) and BBW 76, for which the limit is rather poor (rms = 0.3 K). The spectra of the six sources with wings are shown in Figure 1; where ^{13}CO data exist, they are shown on the same plot. Four of the souces show double-peaked profiles. In V1515 Cyg, the ^{13}CO line indicates that these are separate velocity components, but the two peaks result from self-absorption in the other three sources. In addition, a C^{18}O profile toward Elias 1-12 indicates that even the ^{13}CO line is somewhat self-reversed.

The inner and outer boundaries of the wings are also marked in Figure 1 and listed in Table 2, along with the rms noise in the spectra and the ambient cloud velocity (v_{lsr}). These were determined by examining a number of spectra in the map and by comparison to the ^{13}CO spectra. The outer boundaries (v_o) were set to be sure to include all the wing emission at every position, while the inner boundaries (v_i) were set to exclude the line core based on either the increase of the CO/^{13}CO ratio above typical ambient cloud levels or on a clear excess over a Gaussian, fitted to the line core.

The contour maps of the wings are shown in Figure 2. For V1057 Cyg and V1515 Cyg, only strip scans could be made, so

TABLE 2

SPECTRAL CHARACTERISTICS

Source	rms (K)	v_{lsr} (km s^{-1})	v_o (blue) (km s^{-1})	v_i (blue) (km s^{-1})	v_i (red) (km s^{-1})	v_o (red) (km s^{-1})
V346 Nor	0.17	−3.1	−19.0	−5.0	−1.0	19.0
V1515 Cyg	0.08	5.7	1.0	4.0		
V1057 Cyg	0.15	8.7	1.0	7.0		
Elias 1-12	0.20	3.9	−10.0	0.0	8.0	17.0
RNO 1b	0.17	−18.4	−40.0	−20.0	−15.0	0.0
FU Ori	0.06	11.8				
Z CMa	0.17	13.7	8.0	12.0	16.0	22.0
BBW 76	0.30	17				

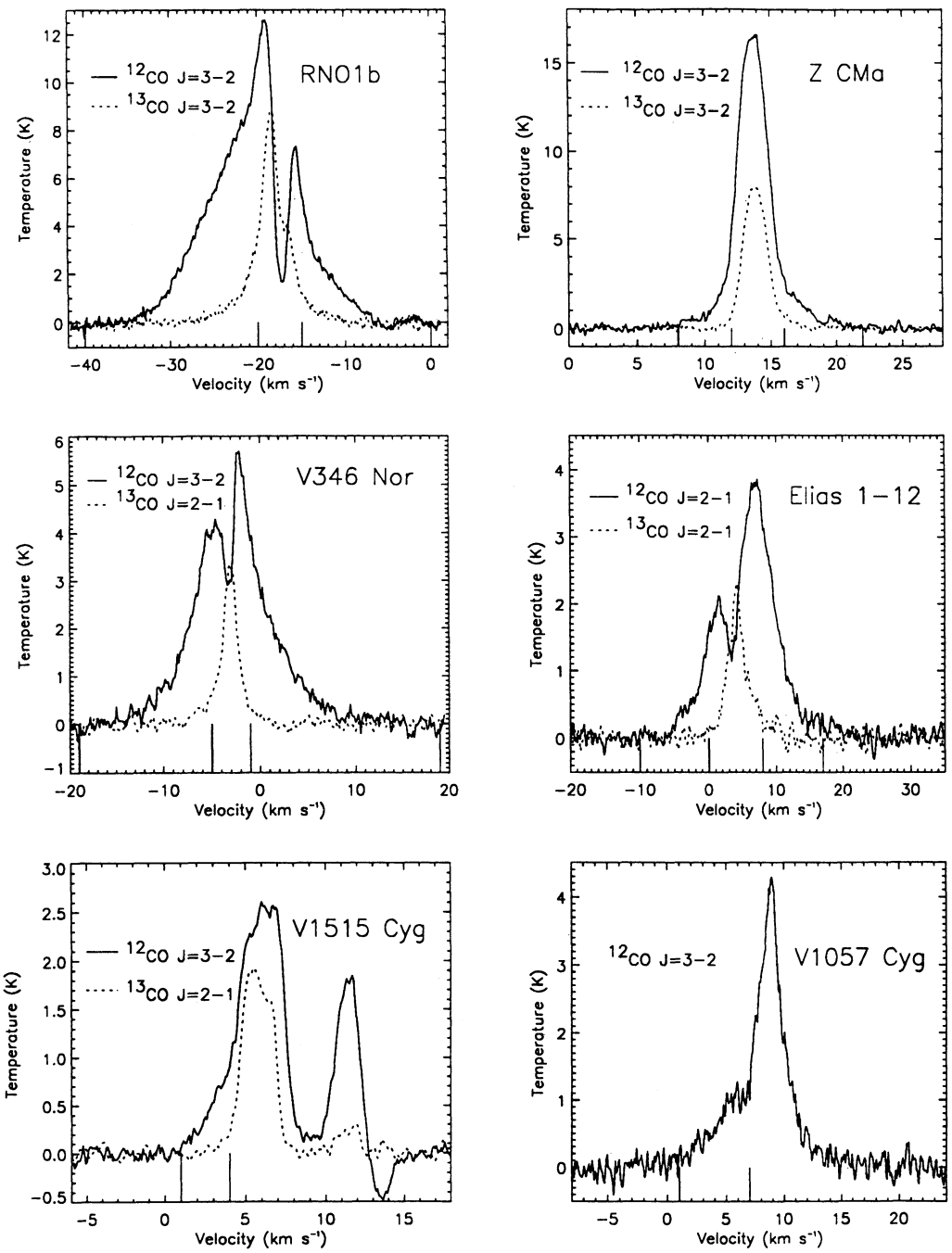

FIG. 1.—Spectra of the (0, 0) positions for all six sources with detected wings. The solid lines are the CO $J = 3 \rightarrow 2$ lines, except for Elias 1-12, for which we show the $J = 2 \rightarrow 1$ line. The dotted lines are ^{13}CO lines, either $J = 3 \rightarrow 2$ or $2 \rightarrow 1$, as indicated in the figure. The vertical scale is T_A^*. The vertical lines along the velocity axes indicate the wing boundaries in Table 2. The dip below zero at a velocity around 13.5 km s^{-1} in the spectrum of V1515 Cyg is caused by emission in the reference position.

no contour maps are presented. Maps of these sources have been made by S. McMuldroch (1993, private communication). In the case of Z CMa, the blue wing peaks at the star's position, with the red wing displaced by 20″ to the northeast. Both lobes are quite compact, roughly 20″–50″ at the FWHM level. Given the weakness of the wings, the beam size, and reasonable pointing uncertainties, the flow could easily originate from the position of the star. In addition, the position angle of the outflow is about 60° (counterclockwise from north), the same as that of a jet and a collection of Herbig-Haro objects which also show blueshifts to the southwest (Poetzel, Mundt, & Ray 1989). All these facts suggest Z CMa as the source of the outflow, but a very close infrared companion (Koresko et al. 1991) is an alternative driving source (see discussion in § 5).

In RNO 1b, the midpoint of the line between the two peaks is about 4″ east and 10″ north of RNO 1b, still consistent with RNO 1b being the driving force, but closer to the positions of IRAS 00338+6312, which is 8″ east and 8″ north of RNO 1b,

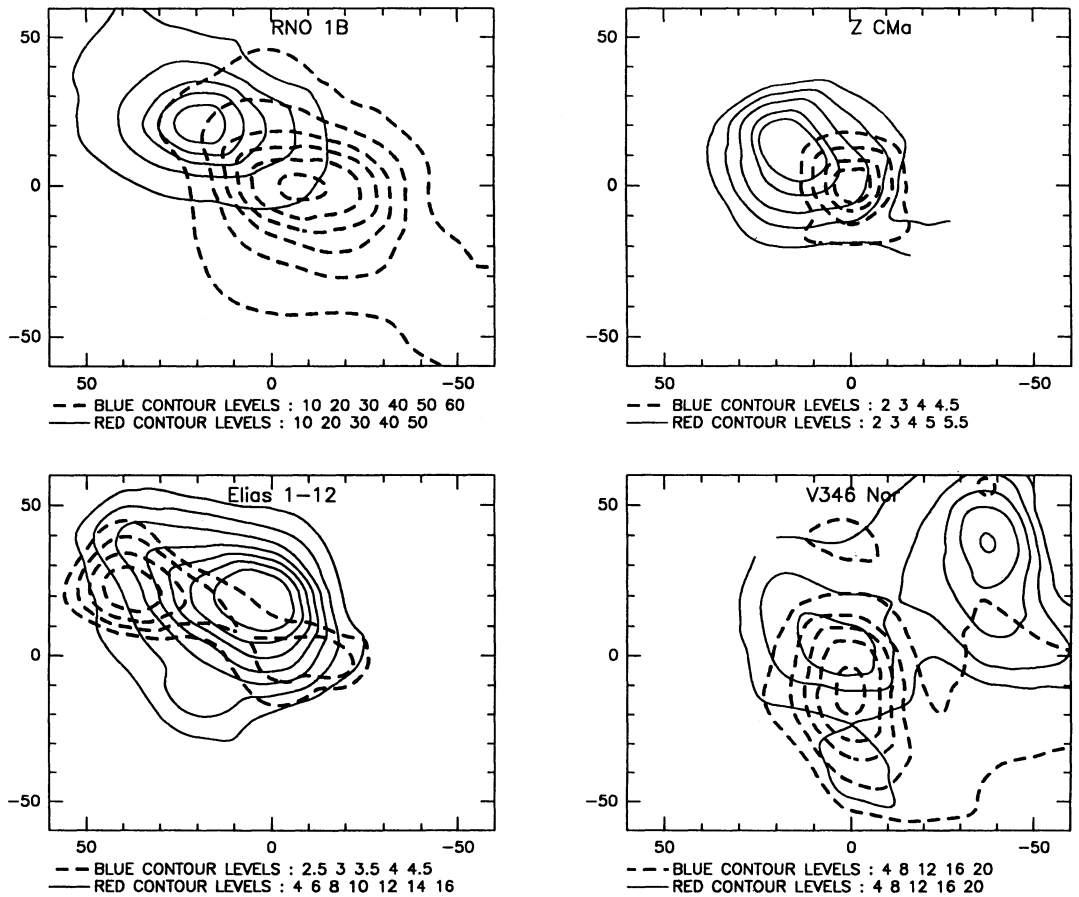

FIG. 2.—Maps of both red (*solid contours*) and blue (*dashed contours*) wings on the $J = 3 \rightarrow 2$ line of CO for the four sources with maps. The axes are offsets from the positions in Table 1, in units of arcsec. The contour levels (K km s^{-1}) are indicated under each figure. The lowest contour level is roughly 30 σ, 7 σ, 10 σ, and 5 σ in RNO 1b, Z CMa, Elias 1-12, and V346 Nor, respectively.

or RNO 1c, which lies midway between 1b and the *IRAS* source. RNO 1c also appears to be an FU Orionis object (Kenyon et al. 1993). The estimated combined luminosity of 1b and 1c is close to the *IRAS* luminosity, but the *IRAS* source may still be powered separately. A water maser has been detected at the position of the *IRAS* source (Menten 1992). The polarization pattern in the region suggests two reflection nebulae, one associated with the *IRAS* source, and one associated with 1b and 1c (Weintraub & Kastner 1993). Therefore, it is unclear which source drives the molecular outflow. This outflow has also been mapped by Yang et al. (1991) in CO $J = 1 \rightarrow 0$. Our map is similar to theirs in shape, including the elongation of the blue lobe, but they find that the red lobe peaks on the *IRAS* source.

The maps of the other two sources are more complex, with evidence for more than one outflow. In the case of Elias 1-12, the stellar position is about 20″ south of the peak of the red wing, and the strongest blue wing peaks 40″ east and 20″ north. There is a weaker blue wing which peaks southwest of Elias 1-12. We interpret this pattern as indicative of an outflow centered on Elias 1-12 and a separate, stronger outflow centered about 20″ east and 20″ north. We consider the two blue lobes separately, but there is no way to separate cleanly the different contributions to the red lobe.

Finally, we consider the map of V346 Nor, which has a still more complicated morphology. There appear to be at least two flows, one centered on the stellar position and one centered about 40″ west, but lacking a clear blue lobe. In addition, there is a weak red lobe south of the star, overlaying the blue lobe and possibly a separate blue lobe north of the star. For the purposes of determining masses, etc., we have used only the contours which center on V346 Nor, ignoring the red peak in the south and the possible blue lobe in the north, as well as the western outflow.

4. ANALYSIS

From the contour maps, the extent of each wing was determined, the integrated intensity was integrated over solid angle, and the integrated column density was calculated from

$$\int N(\mathrm{CO}) d\Omega = \frac{1.104 \times 10^{15}\ \mathrm{cm}^{-2}\ \mathrm{sr}}{D(n, T)} \frac{\iint T_A^* \, dv \, d\Omega}{\eta_{\mathrm{mb}}} \frac{\tau_{23}}{1 - e^{-\tau_{23}}}, \quad (1)$$

where T_A^* has units of K km s^{-1}, τ_{23} is the optical depth in the $J = 3 \rightarrow 2$ line, η_{mb} is the main beam efficiency, and $D(n, T)$ is given by

$$D(n, T) = f_2[J(T_{\mathrm{ex}}) - J(T_{\mathrm{bk}})](1 - e^{-16.6/T_{\mathrm{ex}}}) . \quad (2)$$

$J(T)$ is the Planck function in temperature units. Choi, Evans, & Jaffe (1993) explain the rationale for this formulation, which

avoids some assumptions required by the usual LTE method, T_{ex} is the excitation temperature of the $J = 3 \rightarrow 2$ transition, f_2 is the fraction of the population in the $J = 2$ level, and T_{bk} is the temperature of the cosmic background radiation. Calculations with LVG codes show that, for column densities typical of outflows, $D(n, T) = 2.0 \pm 0.7$ for densities between 10^4 cm^{-3} and 10^6 cm^{-3} and temperatures between 15 K and 100 K (Choi et al. 1993). We have assumed $D(n, T) = 2.0$ in all further calculations.

The optical depth correction factor (the last factor in eq. [1]) was averaged over each line wing, weighted by the intensity of the CO emission. For each velocity, τ_{23} was determined from the ratio of CO and ^{13}CO lines, assuming equal excitation temperatures and a local abundance ratio (CO/^{13}CO) of 57 (Langer & Penzias 1990). These ratios were generally obtained at the (0, 0) position, except for the red wing of RNO 1b and the blue wing of Elias 1-12, for which spectra at the peak of the wing were used. For Z CMa and RNO 1b, $J = 3 \rightarrow 2$ lines were used for both CO and ^{13}CO. For Elias 1-12, the $J = 2 \rightarrow 1$ lines were used for both and τ_{23} was assumed equal to τ_{12}. Excitation calculations similar to those of Choi et al. (1993) show that $0.6 < \tau_{23}/\tau_{12} < 1.4$ for 10 K $< T <$ 30 K and 10^4 cm^{-3} $< n < 10^6$ cm^{-3}, conditions typical in outflows. For V346 Nor, we had available only $J = 3 \rightarrow 2$ lines from CO and $J = 2 \rightarrow 1$ lines from ^{13}CO, so we also had to assume equal excitation temperatures in the two transitions. Since the correction for optical depth depends on a number of assumptions, we have also derived results which assumed $\tau_{23} \ll 1$, providing a lower limit on the integrated column densities, and thus all quantities derived from them. The values for this case are given first in Table 3, followed by those with optical depth corrections, and the average optical depth (weighted by intensity) is given in column (5).

Given values for the integrated column densities, we calculated the masses in each lobe from

$$M = \frac{\mu m_H d^2 \int N(\mathrm{CO}) d\Omega}{X(\mathrm{CO})}, \quad (3)$$

where $\mu = 2.3$ is the mean molecular weight, m_H is the mass of hydrogen atom, d is the distance to the source, and X(CO) is the CO abundance, assumed to be 1×10^{-4} (van Dishoeck et al. 1992). The results are tabulated in Table 3, where we give masses for each lobe and M_{tot}, the sum of the two lobes. The total masses range from a low of 0.07 $M_\odot$ (Z CMa) to a high of 0.44 $M_\odot$ (RNO 1b) without optical depth corrections. With optical depth corrections, the range is 0.37–4.5 $M_\odot$.

The momentum of the outflow is given by

$$P = \int M(v) v \, dv \sim M \frac{v_o + v_i}{2}, \quad (4)$$

where v_o and v_i are now taken relative to v_{lsr}, the cloud ambient velocity. Likewise, the energy in the flow is given by

$$E = \int \frac{1}{2} M(v) v^2 \, dv \sim \frac{M}{2} \frac{v_o^2 + v_o v_i + v_i^2}{3}, \quad (5)$$

The dynamical time of the flow (t) is calculated by dividing the maximum size of the flow by the maximum velocity in the wing. Finally, the mass-loss rate, averaged over the dynamical time, is calculated from

$$\dot{M} = \frac{P}{t v_{wind}}, \quad (6)$$

where v_{wind} is the stellar wind velocity, assumed to be 300 km s^{-1} (see, e.g. Levreault 1988a). In the absence of information on the inclination of these outflows, we have made no corrections for inclination. Consequently, we may be underestimating the momentum and energy. The approximations in equations (4) and (5) can cause us to overestimate the momentum and energy by a similar amount. Inclination effects will cause us to overestimate the lifetime of the flow if it lies in the plane of the sky and to underestimate the lifetime if the flow is face-on. Further discussion of the uncertainties in these estimates can be found in Levreault (1988b) and Choi et al. (1993).

The results of these calculations are found in Table 4. Our values of $\dot{M}$ are compared to those of previous studies, where available. The sum of the $\dot{M}$ from the two lobes ranges from 3.3×10^{-8} (Z CMa) to 2.2×10^{-6} $M_\odot$ yr^{-1} (RNO 1b) with the optically thin assumption. The former is comparable to the smallest $\dot{M}$ in the sample of Levreault (1988a) of young, low-mass stars, while the latter is comparable to the largest value in the sample. With optical depth corrections, the numbers are larger by a factor of 5 on average.

We have followed the traditional method for estimating lifetimes and thus mass-loss rates in outflows, but we note that Parker, Padman, & Scott (1991) have argued that the lifetimes obtained from this method are inconsistent with the statistics of outflow detections. If the outflow is stationary, it may be much older than the dynamical time (e.g., Dyson, Cantó, & Rodríguez 1988; Masson & Chernin 1993). The dynamical times in Table 4 are typically 10^4 yr, about an order of magnitude less than the average lifetime of 2×10^5 yr deduced by

TABLE 3

OUTFLOW MASSES

Source (1)	Distance (pc) (2)	Wing (3)	$\iint T_A^* dv \, d\Omega$ (K km s^{-1} sr) (4)	τ (5)	M ($M_\odot$) (6)	M_{tot} ($M_\odot$) (7)
V346 Nor	620	Blue	7.2 (−7)	Thin; 6.0	0.05; 0.3	
	620	Red	5.0 (−7)[a]	Thin; 1.5	0.03; 0.07	0.08; 0.37
Elias 1-12	900	Blue	1.2 (−7)[b]	Thin; 3.1	0.017; 0.06	
	900	Red	9.5 (−7)	Thin; 2.5	0.14; 0.38	0.16; 0.44
RNO 1b	850	Blue	3.1 (−6)	Thin; 9.2	0.4; 3.7	
	850	Red	1.8 (−6)	Thin; 3.1	0.2; 0.8	0.6; 4.5
Z CMa	1150	Blue	7.1 (−8)	Thin; 6.6	0.02; 0.11	
	1150	Red	2.2 (−7)	Thin; 14	0.05; 0.71	0.07; 0.82

[a] Includes only the lobe centred near 0, 0; the lobe centered near −40, 40 has a value of 8.3×10^{-7} K km s^{-1} sr.
[b] Including only the lobe centered at −10, 0; the lobe centered at 40, 20 has a value of 1.6×10^{-7} K km s^{-1} sr.

TABLE 4

MASS-LOSS RATES

Source	Wing	P ($M_\odot$ km s^{-1})	E (ergs)	t (yr)	$\dot{M}$ ($M_\odot$ yr^{-1})	$\dot{M}$ (pub) ($M_\odot$ yr^{-1})
V346 Nor	Blue	0.44	4.6 (43)	1.0 (4)	1.5 (−7)	
		2.6	2.8 (44)	...	8.8 (−7)	
	Red	0.42	6.1 (43)	6.1 (3)	2.3 (−7)	
		0.82	1.2 (44)	...	4.5 (−7)	
Elias 1-12	Blue	0.16	1.6 (43)	8.8 (3)	6.1 (−8)	
		0.52	5.1 (43)	...	2.0 (−7)	
	Red	1.2	1.1 (44)	2.4 (4)	1.6 (−7)	1.1 (−7)[a]
		3.3	3.1 (44)	...	4.5 (−7)	
RNO 1b	Blue	4.6	6.7 (44)	1.1 (4)	1.4 (−6)	6.7 (−7)[b]
		43	6.2 (45)	...	1.3 (−5)	
	Red	2.5	3.2 (44)	1.0 (4)	8.4 (−7)	4.8 (−7)[b]
		8.4	1.1 (45)	...	2.8 (−6)	
Z CMa	Blue	0.09	5.2 (42)	2.4 (4)	1.2 (−8)	
		0.6	3.5 (43)	...	8.2 (−8)	
	Red	0.19	7.8 (42)	3.1 (4)	2.1 (−8)	
		2.6	1.1 (44)	...	2.8 (−7)	

[a] Levreault 1988a.

[b] Calculated from the P and t given in Yang et al. (1991), assuming $v_{\rm wind} = 300$ km s^{-1}.

Parker et al. on statistical grounds. If Parker et al. are right, and if these objects are typical, we would be overestimating the mass-loss rates by about an order of magnitude. The case is by no means closed. Natta & Giovanardi (1990) found excellent agreement between mass-loss rates derived from CO by the traditional method and rates they derived from Na I lines.

The mass-loss rates are subject to considerable uncertainty, the largest of which arise from difficulties in defining boundaries of the flow and identification of the driving source in some cases. Uncertainties about optical depth corrections and the flow lifetime are probably the next most important sources of error, followed by inclination effects. Uncertainties about the excitation and approximations made in the equations are probably the least important.

5. DISCUSSION

5.1. *Comparison with Previous Results*

A comparison of our results with those obtained in previous studies can provide a check on our calculations. Levreault (1988b) found only the red wing toward Elias 1-12 strong enough to map; he assumed the wings to be optically thin and found a mass and dynamical time about twice ours (probably a result of his lower resolution) and derived an $\dot{M}$ about 70% of ours, assuming $\tau_{23} \ll 1$. Thus our results are in good agreement with results using a similar method. With optical depth corrections, we derive an $\dot{M}$ 4 times larger than Levreault, but more importantly, our map, with higher spatial resolution, suggests that this red wing arises at least in part from a different flow. Thus it may be more appropriate to use only the blue flow located southeast of the star in assessing the $\dot{M}$ for the star. If we assume an equal $\dot{M}$ contribution in the red wing, and double the blue wing rate, we get an $\dot{M}$ of 1–4 × 10^{-7} $M_\odot$ yr^{-1} for Elias 1-12. For comparison, Rodríguez & Hartmann (1992) found radio continuum emission from Elias 1-12 (and V1057 Cyg) which was consistent with thermal free-free emission from an ionized wind with $\dot{M} \sim 10^{-7}$ $M_\odot$ yr^{-1}, a lower limit to $\dot{M}$ since the wind may be only partially ionized.

Levreault (1988b) also observed Z CMa but did not detect an outflow; this is not surprising given the weakness of the wings and the compactness of the flow. Indeed, with the eye of hindsight, very weak wings can be seen on his spectrum. The outflow age in Z CMa is 2–3 × 10^4 yr, but since the flow is barely resolved, the age estimate is quite uncertain. Interestingly, Herbig-Haro objects are seen at much larger distances from the star (up to 6′) than is the CO emission, but they are also moving much faster. Poetzel et al. (1989) derive dynamical times of 2–3 × 10^4 yr for the slow knots, similar to our estimates.

The outflow in RNO 1b has been mapped in the $J = 1 \rightarrow 0$ line of CO by Yang et al. (1991). If we used their values of P and t, we would calculate $\dot{M}$ for RNO 1b which are about half the values we find for both lobes, before we correct for optical depth. With optical depth corrections, the discrepancy worsens to factors of 6 (red lobe) and 20 (blue lobe). Since the dynamical times we derive are similar to theirs, the difference is in the lower masses that they derived. Our integrated intensities are considerably larger than theirs, partly because they included a much smaller range of velocities in the wing and partly because our wings are much stronger (compare Fig. 1 with their Fig. 2). At any rate, the relevance of this outflow to the FU Orionis star is unclear, as discussed above.

5.2. *The Case of Z CMa*

Z CMa has usually been classified as a Herbig Ae/Br star, but Hartmann et al. (1989) argued that its spectrum was best understood as that of an FU Orionis object. More recently, Koresko et al. (1991) showed that the optical component of Z CMa could be an FU Orionis star with the typical luminosity of such stars, while most of the luminosity arose in the infrared companion. Furthermore, Whitney et al. (1993) interpreted spectropolarimetry in terms of a model with both an FU Orionis star and a more extincted Herbig Ae/Be star, whose spectrum is seen primarily in scattered (and hence polarized) light. The contribution from the Ae/Be star is quite variable, either because of intrinsic variations or because of variations in the scattering envelope. This model explains why the star was historically classified as a Herbig Ae/Be star and why an emission-line spectrum dominated when the system was bright (Hessman et al. 1991), while spectra during faint periods indicate an F star.

Our observations cannot distinguish which of the two stars drives the outflow. On statistical grounds, the FU Orionis star

is a viable candidate, since we find a high percentage to have outflows. There are no complete surveys of Herbig Ae/Be stars for outflows, but the existing, partial surveys have detection rates of 25% to 43% (Cantó et al. 1981, 1984; Levreault 1988a). The optical tracers of mass loss clearly apply to the FU Orionis object, so the following calculation is correct only if the FU Orionis object drives the molecular outflow. The Hα line has wings extending to 1000 km s^{-1}; if we use this velocity in equation (6), we would get a total $\dot{M} \sim 10^{-8}\ M_\odot\ yr^{-1}$ without corrections for optical depth and about $10^{-7}\ M_\odot\ yr^{-1}$ with the large, but rather uncertain, corrections found for this source. Dividing these numbers by the current mass-loss rate of $10^{-5}\ M_\odot\ yr^{-1}$ (Hartmann et al. 1989) gives a duty cycle of 10^{-3} to 10^{-2}, assuming that all the mass loss arises from outbursts from the FU Orionis object.

6. CONCLUSIONS

We have detected molecular outflows toward six out of eight FU Orionis objects, suggesting that these objects commonly produce outflows. However, there are uncertainties in assigning mass-loss rates to the FU Orionis stars. There are multiple outflows in at least two cases of the four that we have fully mapped. In the other two cases, with only one obvious outflow, there are multiple sources and the FU Orionis object may not be the driving source of the outflow. In addition, optical depth corrections are uncertain and questions have been raised about the standard method of computing mass-loss rates from molecular outflows.

Because of all these uncertainties, it is difficult to draw firm conclusions. Nevertheless, two general points can be made. First, the idea of repetitive FU Ori outbursts is consistent with the observations. Most of the sources have outflows in their vicinity, and as pointed out in the Introduction, these outflows are too big to have originated in the most recent outburst, pointing to a previous episode of mass ejection. We also note that the two objects in our sample without detectable outflows, FU Ori and BBW 76, are also the objects with the smallest far-infrared excesses (Kenyon & Hartmann 1991); the other FU Ori objects are either heavily extincted or have large excesses at $\lambda \gtrsim 10\ \mu m$. FU Ori and BBW 76 could have originally had outflows which eventually dispersed their remnant envelopes, explaining the lack of detectable swept-up material which constitutes molecular outflows.

Second, FU Ori outbursts can easily provide the required momentum fluxes with a relatively small duty cycle. If one adopts the peak mass-loss of FU Ori of about $10^{-5}\ M_\odot\ yr^{-1}$ (Croswell et al. 1987; Calvet et al. 1993), then the time-averaged mass-loss rates in Table 4 suggest duty cycles of 10^{-3} to 10^{-1}, with the lowest values applying with no optical depth corrections to Z CMa, and the largest to V346 Nor with optical depth corrections. The only exception to this is RNO 1b, and as pointed out above this outflow may be dominated by another, more luminous, source. Kenyon, Calvet, & Hartmann (1993) argue that the duty cycle of FU Ori outbursts during the embedded phase is ~5% based on crude statistics available in Taurus. We conclude that FU Ori outbursts with a duty cycle of about 0.01 can produce outflows with time-averaged mass outflow rates $\sim 10^{-7}\ M_\odot\ yr^{-1}$, similar to the range of mass-loss rates that we observe.

We would like to thank C. E. Walker and Y. Wang for collecting some of the data for this paper. We also thank M. Choi for assistance with some of the analysis and an anonymous referee for helpful suggestions. The research was supported in part by NSF grant AST 90-17710, by a grant from the Keck Foundation, and by a grant from the Texas Advanced Research Program to the University of Texas at Austin.

REFERENCES

Bell, K. R., & Lin, D. N. C., 1993, ApJ, submitted
Calvet, N., Hartmann, L., & Kenyon, S. J. 1993, ApJ, 402, 623
Cantó, J., Rodríguez, L. F., Barral, J. F., & Carral, P. 1981, ApJ, 244, 102
Cantó, J., Rodríguez, L. F., Calvet, N., & Levreault, R. 1984, ApJ, 282, 631
Choi, M., Evans, N. J., II, & Jaffe, D. T. 1993, ApJ, 417, 624
Croswell, K., Hartmann, L., & Avrett, E. H. 1987, ApJ, 312, 227
Dyson, J. E., Cantó, J., & Rodríguez, L. F. 1988, in Mass Outflows from Stars and Galactic Nuclei, ed. L. Bianchi & R. Gilmozzi (Dordrecht: Kluwer), 299
Hartmann, L., Kenyon, S. J., & Hartigan, P. 1993, in Protostars and Planets III, ed. E. H. Levy & J. Lunine (Tucson: Univ. Arizona), 497
Hartmann, L., Kenyon, S. J., Hewett, R., Edwards, S., Strom, K. M., Strom, S. E., & Stauffer, J. R. 1989, ApJ, 338, 1001
Hessman, F. V., Eisloeffel, J., Mundt, R., Hartmann, L. W., Herbst, W., & Krautter, J. 1991, ApJ, 370, 384
Kenyon, S. J., Calvet, N., & Hartmann, L. 1993, ApJ, 414, 676
Kenyon, S. J., & Hartmann, L. 1991, ApJ, 383, 664
Kenyon, S. J., Hartmann, L., Gomez, M., Carr, J., & Tokunaga, A. 1993, AJ, 105, 1505
Kenyon, S. J., Hartmann, L., & Hewitt, R. 1988, ApJ, 325, 231
Koresko, C. J., Beckwith, S. V. W., Ghez, A. M., Matthews, K., & Neugebauer, G. 1991, AJ, 102, 2073
Langer, W. D., & Penzias, A. A. 1990, ApJ, 357, 477
Levreault, R. M. 1988a, ApJ, 330, 897
———. 1988b, ApJS, 67, 283
Mangum, J. 1993, PASP, 105, 117
Masson, C. R., & Chernin, L. M. 1993, ApJ, 414, 230
Menten, K. 1992, private communication
Natta, A., & Giovanardi, C. 1990, ApJ, 356, 646
Parker, N. D., Padman, R., & Scott, P. F. 1991, MNRAS, 252, 442
Poetzel, R., Mundt, R., & Ray, T. P. 1989, A&A, 224, L13
Reipurth, B. 1990, in IAU Symp. 136, Flare Stars in Star Clusters, Associations, and the Solar Vicinity, ed. L. V. Mirzoyan, B. R. Pettersen, & M. K. Tsvetkov (Dordrecht: Kluwer), 229
Rodríguez, L. F., & Hartmann, L. 1992, Rev. Mexicana Astron. Af., 24, 135
Staude, H. J., & Neckel, Th. 1992, ApJ, 400, 556
Strom, K. M., & Strom, S. E. 1993, ApJ, 412, L63
van Dishoeck, E. F., Glassgold, A. E., Guelin, M., Jaffe, D. T., Neufeld, D., Tielens, A. G. G. M., & Walmsley, C. M. 1992, in IAU Symp. 150, Astrochemistry of Cosmic Phenomena, ed. P. D. Singh (Dordrecht: Kluwer), 285
Weintraub, D. A., & Kastner, J. H. 1993, ApJ, 411, 767
Whiteny, B. A., Clayton, G. C., Schulte-Ladbeck, R. E., Calvet, N., Hartmann, L., & Kenyon, S. J. 1993, ApJ, submitted
Yang, J., Umemoto, T., Iwata, T., & Fukui, Y. 1991, ApJ, 373, 137